

## Kinetic selection of Pd<sub>4</sub>L<sub>2</sub> metallocyclic and Pd<sub>6</sub>L<sub>3</sub> trigonal prismatic assemblies

Helen M. O'Connor, Marco Coletta, Alvaro Etcheverry-Berríos, Gary S. Nichol, Euan K. Brechin\* and Paul J. Lusby\*

### Table of Contents

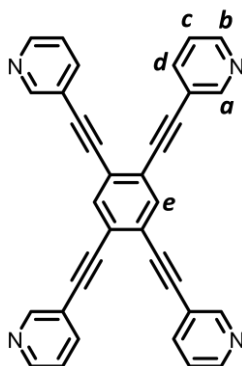
S1. Materials and Methods.....	2
S2. Synthesis.....	2
S2.1.1 Synthesis of 1,2,4,5-tetra(pyridin-3-ylethynyl)benzene ( <b>L</b> <sup>T</sup> ).....	2
S2.1.2 Synthesis of [(TMEDA)PdCl <sub>2</sub> ].....	3
S2.1.3 Synthesis of <b>1a</b> ·OTf and <b>1b</b> ·OTf.....	3
S2.1.4 Synthesis of <b>2</b> ·OTf.....	4
S2.1.5 Synthesis of <b>2</b> ·BARF.....	5
S2.2.1 Spectroscopic data for <b>L</b> <sup>T</sup> .....	6
S2.2.2 Spectroscopic data for <b>1a</b> ·OTf and <b>1b</b> ·OTf.....	7
S2.2.3 Spectroscopic data for <b>2</b> ·OTf.....	8
S2.2.4 Comparison of spectroscopic data for <b>2</b> ·OTf, <b>L</b> <sup>T</sup> and [(dppp)Pd(OTf) <sub>2</sub> ].....	9
S2.2.5 Time dependent <sup>1</sup> H NMR spectra of <b>2</b> ·OTf.....	10
S2.2.6 <sup>1</sup> H NMR spectrum of the anion metathesis reaction of <b>1a</b> ·OTf and <b>1b</b> ·OTf with NaBARF.....	10
S2.2.7 Spectroscopic data for <b>2</b> ·BARF.....	11
S3. Mass Spectrometry.....	12
S3.1 Spectroscopic data for <b>1a</b> ·OTf and <b>1b</b> ·OTf.....	12
S3.2 Spectroscopic data for <b>2</b> ·OTf.....	13
S4. Crystallographic Data Analysis.....	15
S4.1 Crystallographic data for <b>L</b> <sup>T</sup> .....	15
S4.2 Crystallographic data for <b>1a</b> ·OTf.....	15
S4.3 Crystallographic data for <b>2</b> ·OTf.....	15
S4.4 Comparison of angles between <b>L</b> <sup>T</sup> and 1,3-bis(pyridine-3-ylethynyl)benzene.....	16
S4.5 Additional crystallographic views.....	17
S4.6 Crystallographic packing.....	19
S4.7 Experimental data for <b>L</b> <sup>T</sup> .....	20
S4.8 Experimental data for <b>1a</b> ·OTf.....	20
S4.9 Experimental data for <b>2</b> ·OTf.....	20
S4.10 Effect of concentration on the growth of single crystals of <b>2</b> ·OTf.....	22
S5. Molecular Modelling.....	23
S5.1 Molecular models for TMEDA-based species.....	23
S5.2 Molecular models for dppp-based species.....	23
S6. Host-Guest Studies.....	24
S7. References.....	26

## S1. Materials and Methods

All reagents and solvents were purchased from Alfa Aesar, VWR, Fluorochem or Sigma Aldrich and used without further purification, unless stated otherwise. All reactions were carried out under air, unless stated otherwise. All  $^1\text{H}$ ,  $^{13}\text{C}$ , and  $^{19}\text{F}$  NMR spectra were recorded on either a 500 MHz Bruker AV III equipped with a DCH cryo-probe (Ava500), a 500 MHz Bruker AV IIIHD equipped with a Prodigy cryo-probe (Pro500), or a 400 MHz Bruker AV III equipped with BBFO+ probe (Ava400), at a constant temperature of 300 K. All DOSY experiments were performed on the Ava500 using bipolar gradient pulses for diffusion with two spoil gradients (ledbpg2s.compensated) pulse sequence. The sequence was carried out under automated conditions where the duration of the magnetic field pulse gradient ( $\delta$ ) was 1.5 ms and the diffusion time ( $\Delta$ ) was 100 ms. Typically, in each PFG NMR experiment, a series of 16 spectra on 32 K data points were collected and the eddy current delay ( $T_e$ ) was set to 5 ms in all experiments. The pulse gradients ( $g$ ) were incremented from 2 to 95% of the maximum gradient strength in a linear ramp. The temperature was set and controlled at 300 K with an air flow of  $400\text{ L h}^{-1}$  in order to avoid any temperature fluctuations due to sample heating during the magnetic field pulse gradients. All  $^1\text{H}$  assignments were made using a combination of COSY and NOESY, unless stated otherwise. Chemical shifts are reported in parts per million. For  $^1\text{H}$  NMR, spectra chemical shifts are referenced to 1.94, 4.33, 5.32, and 7.26 for acetonitrile- $d_3$ , nitromethane- $d_3$ , methylene chloride- $d_2$ , and chloroform- $d$ , respectively. For  $^{13}\text{C}$  NMR spectra, chemical shifts are referenced to 118.26, 62.87, 53.84, and 77.16 for acetonitrile- $d_3$ , nitromethane- $d_3$ , methylene chloride- $d_2$ , and chloroform- $d$ , respectively. Apparent multiplicities are reported using the following standard abbreviations: m = multiplet, q = quartet, t = triplet, d = doublet, s = singlet, bs = broad singlet. All NMR spectroscopic analysis was performed with MestReNova, Version 14.

## S2. Synthesis

### S2.1.1 Synthesis of 1,2,4,5-tetra(pyridin-3-ylethynyl)benzene ( $\text{L}^\dagger$ )



To a solution of 1,2,4,5-tetrabromobenzene (3.942 g, 10 mmol) and 3-ethynylpyridine (4.951 g, 48 mmol) in degassed triethylamine (150 mL) was added bis(triphenylphosphine)palladium(II) dichloride (0.702 g, 10 mol%) and copper(I) iodide (0.286 g, 15 mol%). The solution was stirred for three days at  $80\text{ }^\circ\text{C}$  under an inert atmosphere, during which time a brown precipitate formed. The solvent was removed *in vacuo* before chloroform (150 mL) was added, and the solution filtered. This solution was washed twice with water (40 mL), the organic layer collected and dried over anhydrous magnesium sulfate, before the solvent was removed *in vacuo*. The solid was suspended in hot acetonitrile before being washed by sonication in acetone, to leave  $\text{L}^\dagger$  as a crystalline yellow-brown product. Yield = 2.411 g, 5

mmol, 50%. Colourless needle-shaped single X-ray quality crystals were grown from slow evaporation of a solution of **L<sup>T</sup>** in dichloromethane and methanol. Crystallographic details are provided in section S4.1.

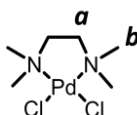
<sup>1</sup>H NMR (500 MHz, CDCl<sub>3</sub>): δ<sub>H</sub> 8.81 (4 H, d, *Ha*), 8.60 (4 H, dd, *Hb*), 7.84 (2 H, s, *He*), 7.83 (4 H, dt, *Hd*), 7.33 (4 H, dd, *Hc*) ppm.

<sup>1</sup>H NMR (500 MHz, CD<sub>2</sub>Cl<sub>2</sub>): δ<sub>H</sub> 8.80 (4 H, broad s, *Ha*), 8.59 (4 H, d, *Hb*), 7.87 (4 H, dt, *Hd*), 7.85 (2 H, s, *He*), 7.34 (4 H, dd, *Hc*) ppm.

<sup>13</sup>C NMR (126 MHz, CD<sub>2</sub>Cl<sub>2</sub>): δ<sub>C</sub> 152.93, 149.96, 138.99, 135.92, 125.82, 123.80, 120.23, 93.14, 90.33 ppm.

<sup>1</sup>H DOSY NMR (500 MHz, CD<sub>2</sub>Cl<sub>2</sub>): 1.03 × 10<sup>-9</sup> m<sup>2</sup> s<sup>-1</sup>, hydrodynamic radius = 5.13 Å.

### S2.1.2 Synthesis of [(TMEDA)PdCl<sub>2</sub>]

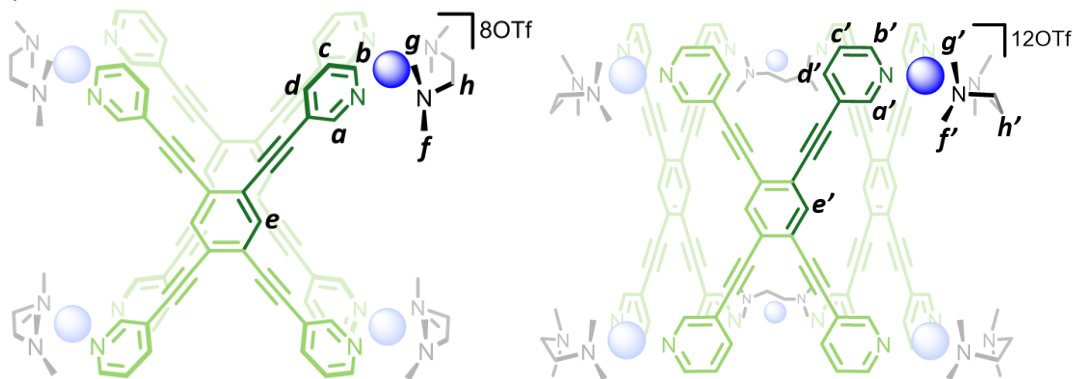


[(TMEDA)PdCl<sub>2</sub>] was prepared according to a modified literature procedure.<sup>1</sup>

To a solution of bis(acetonitrile)dichloropalladium(II) (1.001 g, 4 mmol) in acetonitrile (50 mL) was added N,N,N',N'-tetramethylethylenediamine (TMEDA) (4.0 mL, 27 mmol) at room temperature. The solution was stirred at 75 °C for four hours before being left to cool overnight. The precipitated yellow solid was collected under vacuum and washed with acetonitrile (3 mL), chloroform (2 mL), and diethyl ether (20 mL). Yield = 1.024 g, 2 mmol, 51%.

<sup>1</sup>H NMR (500 MHz, CD<sub>3</sub>NO<sub>2</sub>): δ<sub>H</sub> 2.79 (4 H, s, *Ha*), 2.73 (12 H, dd, *Hb*) ppm.

### S2.1.3 Synthesis of **1a**·OTf and **1b**·OTf



To a solution of [(TMEDA)PdCl<sub>2</sub>] (59 mg, 200 μmol) in water (100 mL) was added silver(I) trifluoromethanesulfonate (110 mg, 430 μmol). The solution was stirred in the dark for two days before the precipitated silver(I) chloride was removed by filtration under gravity. The solvent was removed *in vacuo* before methanol (3 x 20 mL) and diethyl ether (3 x 20 mL) were added and subsequently removed

*in vacuo* to further dry the solid. To a suspension of  $L^T$  (48 mg, 100  $\mu\text{mol}$ ) in nitromethane (50 mL) was added  $[(\text{TMEDA})\text{Pd}(\text{OTf})_2]$  (85 mg, 160  $\mu\text{mol}$ ) in nitromethane (50 mL). The solution was stirred for 36 hours before it was filtered through ceolite. The volume of the solution was reduced to approximately 3 mL *in vacuo* before diethyl ether (20 mL) was added to precipitate an off-white solid which was collected under gravity. Total yield of **1a**·OTf and **1b**·OTf based on  $\text{Pd}'_6L^T_3 = 32$  mg, 7  $\mu\text{mol}$ , 7%. Colourless needle-shaped single X-ray quality crystals were grown from slow diffusion of diethyl ether into an aliquot of the reaction mixture, after 5 days.

#### 1a·OTf

$^1\text{H}$  NMR (500 MHz,  $\text{CD}_3\text{NO}_2$ ):  $\delta_{\text{H}}$  9.35 (8 H, s, Ha), 9.17 (8 H, d, Hb), 8.20 (4 H, s, He), 8.13 (8 H, dt, Hd), 7.70 (8 H, dd, Hc), 3.20 (16 H, bs, Hh), 2.94 (24 H, bs, Hf), 2.81 (24 H, bs, Hg) ppm.

$^{19}\text{F}$  NMR (471 MHz,  $\text{CD}_3\text{NO}_2$ ):  $\delta_{\text{F}}$  -79.21 ppm.

$^1\text{H}$  DOSY NMR (500 MHz,  $\text{CD}_3\text{NO}_2$ ):  $2.80 \times 10^{-10} \text{ m}^2 \text{ s}^{-1}$ , hydrodynamic radius = 11.47 Å.

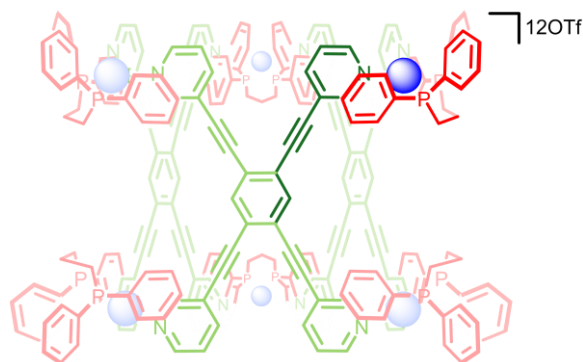
#### 1b·OTf

$^1\text{H}$  NMR (500 MHz,  $\text{CD}_3\text{NO}_2$ ):  $\delta_{\text{H}}$  9.41 (12 H, s, Ha'), 9.26 (12 H, d, Hb'), 8.35 (6 H, s, He'), 8.19 (12 H, dt, Hd'), 7.76 (12 H, dd, Hc'), 3.20 (24 H, bs, Hh'), 2.92 (36 H, bs, Hf'), 2.79 (36 H, bs, Hg') ppm.

$^{19}\text{F}$  NMR (471 MHz,  $\text{CD}_3\text{NO}_2$ ):  $\delta_{\text{F}}$  -79.21 ppm.

$^1\text{H}$  DOSY NMR (500 MHz,  $\text{CD}_3\text{NO}_2$ ):  $3.02 \times 10^{-10} \text{ m}^2 \text{ s}^{-1}$ , hydrodynamic radius = 12.37 Å.

#### S2.1.4 Synthesis of 2·OTf



To a suspension of  $L^T$  (48 mg, 0.10 mmol) in acetonitrile (60 mL) was added  $[(\text{dppp})\text{Pd}(\text{OTf})_2]$  (163 mg, 0.20 mmol) in acetonitrile (60 mL). The solution was stirred for 3 days before it was filtered through ceolite, and the solvent removed *in vacuo* to approximately 5 mL. Diethyl ether (30 mL) was used to precipitate a yellow solid which was collected under gravity. Yield based on  $\text{Pd}'_6L^T_3 = 177$  mg, 0.03 mmol, 30%. Colourless needle-shaped single X-ray quality crystals were grown from slow diffusion of diethyl ether into a 0.3 mM solution of the complex in acetonitrile after 7 days (see Figure S4.9).

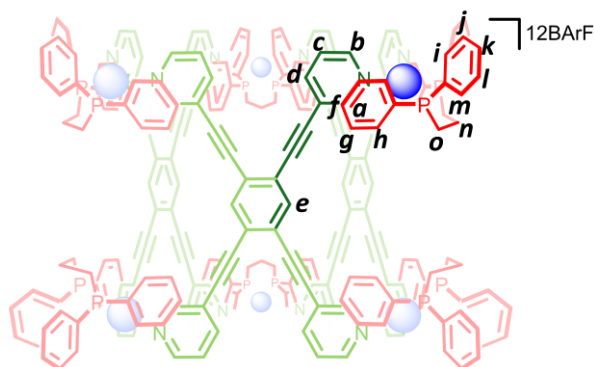
$^1\text{H}$  NMR (500 MHz,  $\text{CD}_3\text{CN}$ ):  $\delta_{\text{H}}$  9.15 (bs), 8.42 (bs), 8.15 (bs), 8.03 (m), 7.75-7.16 (m), 3.52 (m), 3.28 (m), 2.85 (m) ppm.

$^{31}\text{P}$  NMR (202 MHz,  $\text{CD}_3\text{CN}$ ):  $\delta_{\text{P}}$  7.61 ppm.

$^{19}\text{F}$  NMR (471 MHz,  $\text{CD}_2\text{Cl}_2$ ):  $\delta_{\text{F}}$  -78.67 ppm.

$^1\text{H}$  DOSY NMR (500 MHz,  $\text{CD}_2\text{Cl}_2$ ):  $5.37 \times 10^{-10} \text{ m}^2 \text{ s}^{-1}$ , hydrodynamic radius = 11.02 Å.

### S2.1.5 Synthesis of 2·BARf



To a suspension of 2-OTf (170 mg, 27  $\mu\text{mol}$ ) in dichloromethane (9 mL) was added sodium tetrakis[3,5-bis(trifluoromethyl)phenyl]borate (369 mg, 420  $\mu\text{mol}$ ). The solution was sonicated for 30 minutes before it was filtered under gravity. The filtrate was removed *in vacuo* before acetonitrile (1 mL) was used to dissolve the product which was precipitated using water (10 mL). The off-white solid was collected under gravity and dried *in vacuo* to give 2·BARf as an off-white powder. Yield based on  $\text{Pd}_6\text{L}_3$  = 92 mg, 6  $\mu\text{mol}$ , 20%.

$^1\text{H}$  NMR (500 MHz,  $\text{CD}_2\text{Cl}_2$ ):  $\delta_{\text{H}}$  8.46 (12 H, d, Hb), 8.33 (12 H, s, Ha), 8.13 (6 H, s, He), 7.72 (24 H, m, Hk and Hm), 7.67 (BARf-H), 7.59 (24 H, m, Hj and Hl), 7.47 (BARf-H), 7.40 (24 H, dd, Hh), 7.34 (24 H, m, Hd and Hi), 7.19 (24 H, dd, Hg), 7.09 (12 H, dd, Hf), 6.94 (12 H, dd, Hc), 3.49 and 2.95 (24 H, broad t, Ho), 2.83 (12 H, broad m, Hn) ppm.

$^{13}\text{C}$  NMR (126 MHz,  $\text{CD}_2\text{Cl}_2$ ):  $\delta_{\text{C}}$  162.87, 162.48, 162.08, 161.68, 153.40, 147.54, 141.41, 135.32, 134.23, 133.41, 132.95, 131.67, 131.27, 130.06, 129.81, 129.57, 129.31, 129.29, 129.06, 128.33, 126.61, 126.16, 124.89, 123.99, 121.83 ppm.

$^{19}\text{F}$  NMR (471 MHz,  $\text{CD}_2\text{Cl}_2$ ):  $\delta_{\text{F}}$  -62.75 (BARf) and -76.91 (residual triflate) ppm.

$^1\text{H}$  DOSY NMR (500 MHz,  $\text{CD}_2\text{Cl}_2$ ):  $2.76 \times 10^{-10} \text{ m}^2 \text{ s}^{-1}$ , hydrodynamic radius = 19.15 Å.

### S2.2.1 Spectroscopic data for **L**<sup>T</sup>

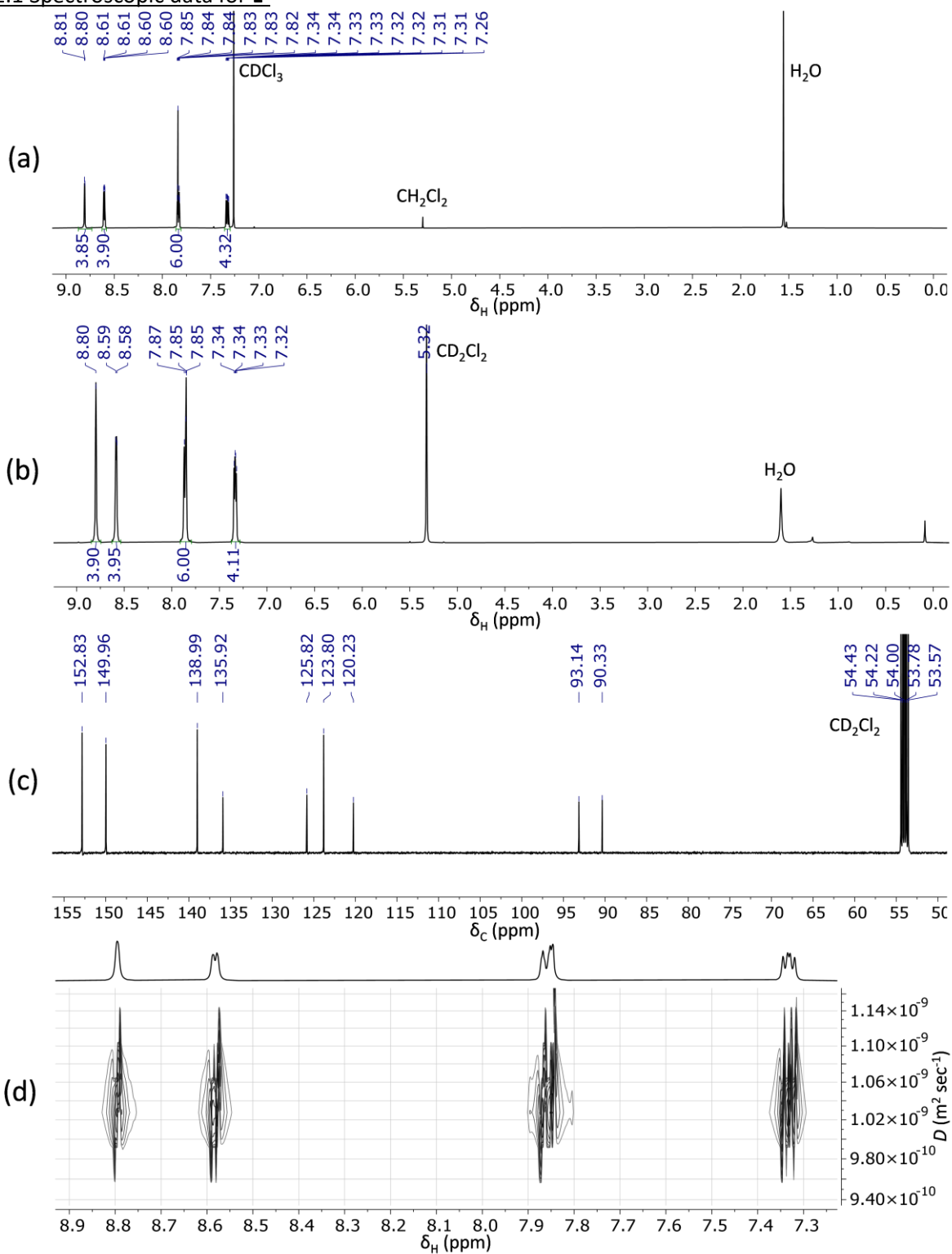


**Figure S2.2.1** (a) <sup>1</sup>H NMR spectrum (CDCl<sub>3</sub>, 500 MHz), (b) <sup>1</sup>H NMR spectrum (CD<sub>2</sub>Cl<sub>2</sub>, 500 MHz), (c) <sup>13</sup>C NMR spectrum (CD<sub>2</sub>Cl<sub>2</sub>, 126 MHz), and (d) <sup>1</sup>H DOSY NMR spectrum (CD<sub>2</sub>Cl<sub>2</sub>, 500 MHz) of **L**<sup>T</sup>.

### S2.2.2 Spectroscopic data for **1a**-OTf and **1b**-OTf

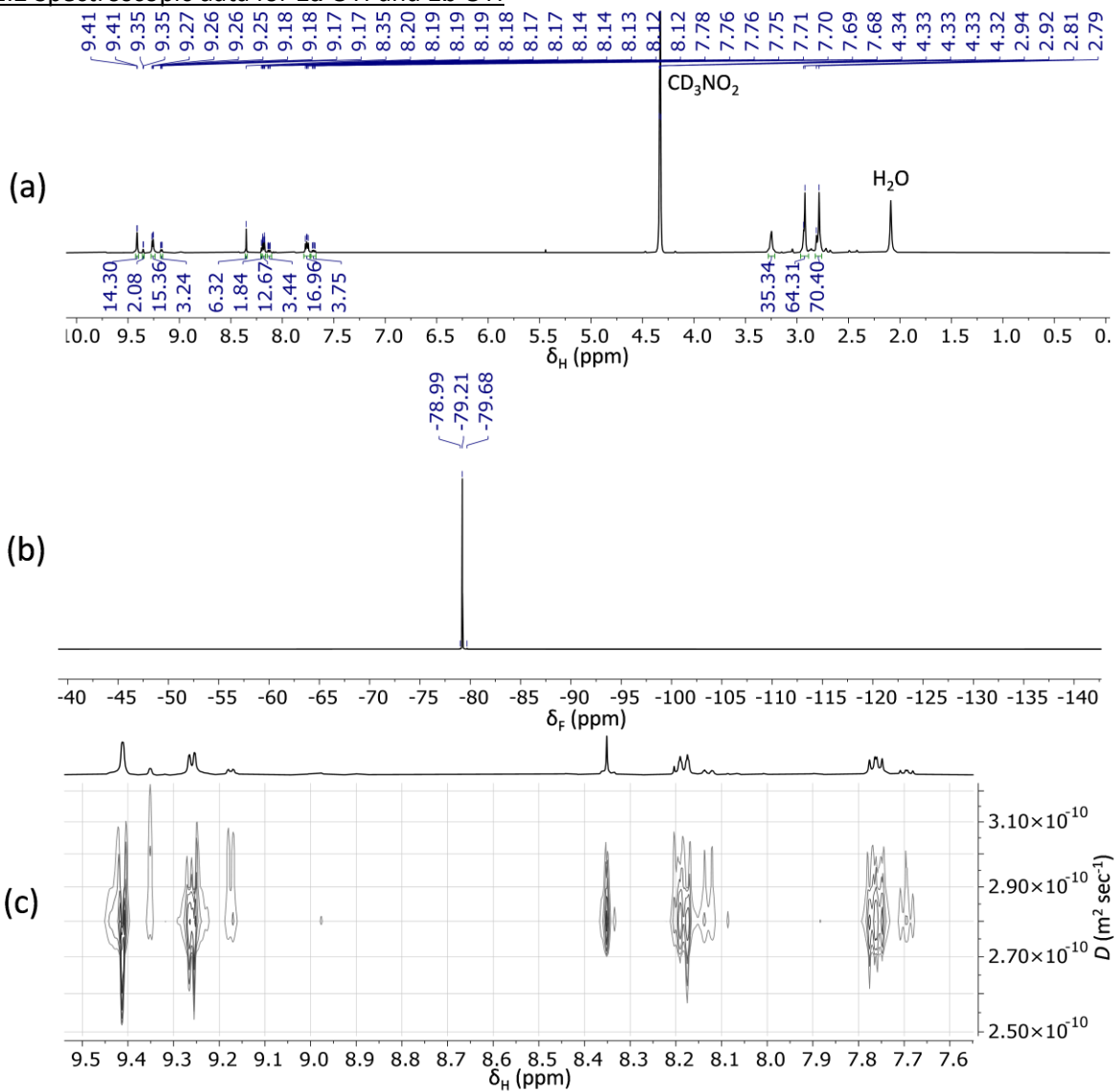


**Figure S2.2.2** (a)  $^1\text{H}$  NMR spectrum ( $\text{CD}_3\text{NO}_2$ , 500 MHz), (b)  $^{19}\text{F}$  NMR spectrum ( $\text{CD}_3\text{NO}_2$ , 471 MHz), and (c)  $^1\text{H}$  DOSY NMR spectrum ( $\text{CD}_3\text{NO}_2$ , 500 MHz) of **1a**-OTf and **1b**-OTf.

### S2.2.3 Spectroscopic data for 2-OTf

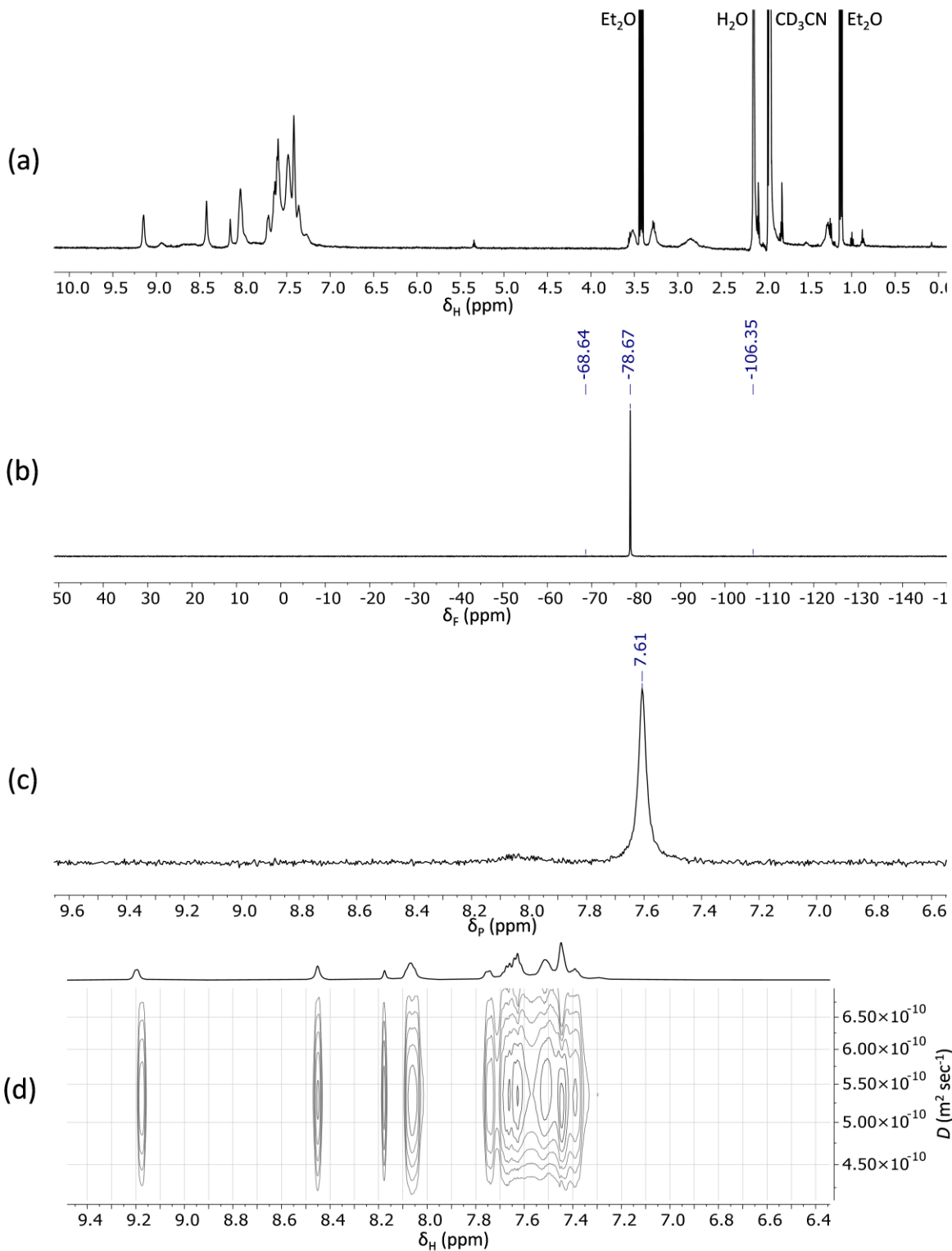


**Figure S2.2.3** (a)  $^1\text{H}$  NMR spectrum ( $\text{CD}_3\text{CN}$ , 500 MHz), (b)  $^{19}\text{F}$  NMR spectrum ( $\text{CD}_3\text{CN}$ , 471 MHz), (c)  $^{31}\text{P}$  NMR spectrum ( $\text{CD}_3\text{CN}$ , 202 MHz), and (d)  $^1\text{H}$  DOSY NMR spectrum ( $\text{CD}_3\text{CN}$ , 500 MHz) of 2-OTf.

### S2.2.4 Comparison of spectroscopic data for **2**·OTf, **L<sup>T</sup>** and **[(dppp)Pd(OTf)<sub>2</sub>]**

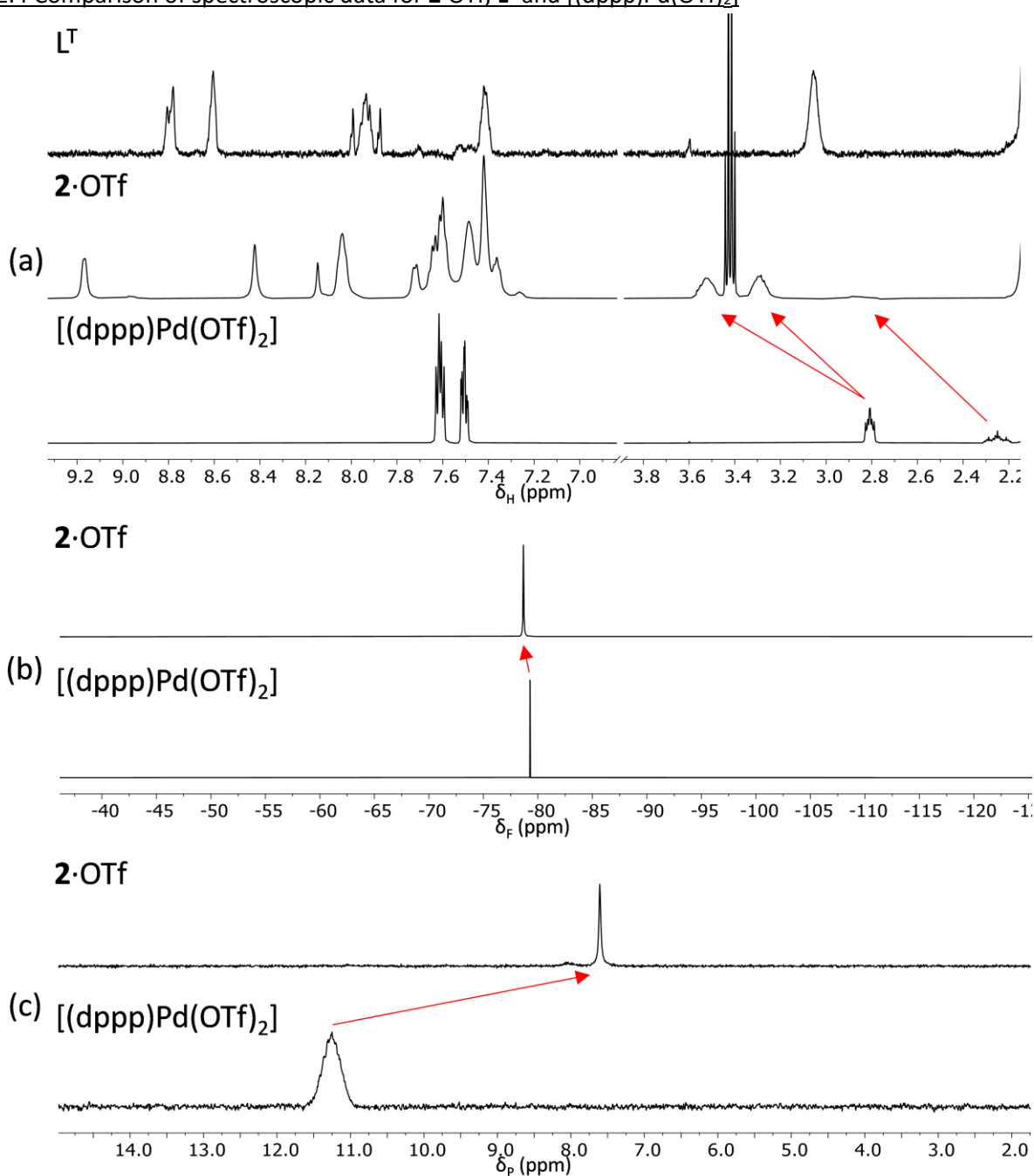


**Figure S2.2.4** (a) Stacked <sup>1</sup>H NMR (CD<sub>3</sub>CN, 500 MHz) spectra of **L<sup>T</sup>** (top), **2**·OTf (middle), and **[(dppp)Pd(OTf)<sub>2</sub>]** (bottom), (b) stacked <sup>19</sup>F NMR spectra (CD<sub>2</sub>Cl<sub>2</sub>, 471 MHz) of **2**·OTf (top), and **[(dppp)Pd(OTf)<sub>2</sub>]** (bottom), and (c) stacked <sup>31</sup>P NMR spectra (CD<sub>3</sub>CN, 202 MHz) of **2**·OTf (top), and **[(dppp)Pd(OTf)<sub>2</sub>]** (bottom). The red arrows indicate shift peaks as a result of coordination to the **[(dppp)Pd(OTf)<sub>2</sub>]** complex.

### S2.2.5 Time dependent $^1\text{H}$ NMR spectra of **2**·OTf

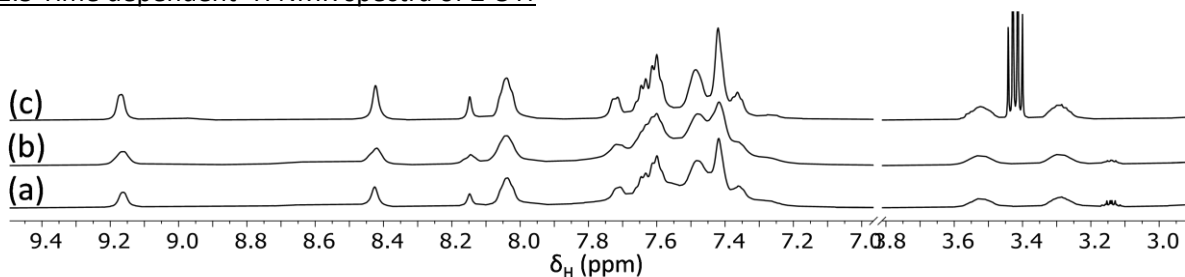


**Figure S2.2.5** Comparison of  $^1\text{H}$  NMR spectra (500 MHz,  $\text{CD}_3\text{CN}$ , 300 K) of **2**·OTf (a) at 10 minutes, (b) at 24 hours, and (c) as an isolated powder obtained after 3 days.

### S2.2.6 $^1\text{H}$ NMR spectrum of the anion metathesis reaction of **1a**·OTf and **1b**·OTf with NaBARf

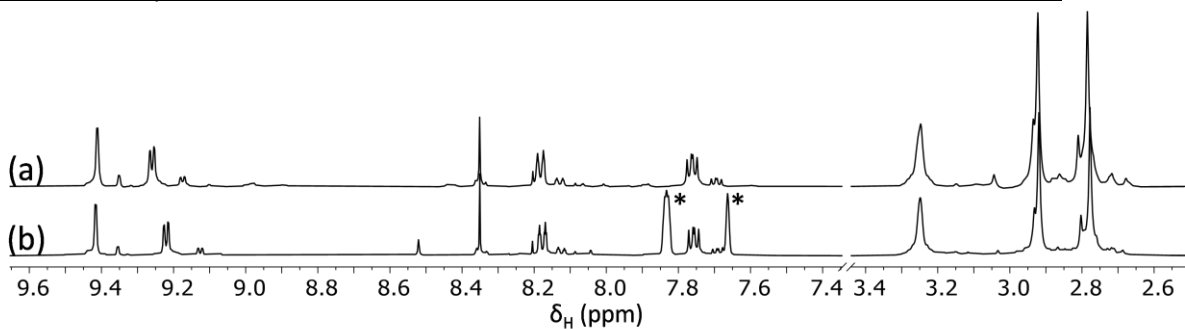


**Figure S2.2.6** Comparison of  $^1\text{H}$  NMR spectra (500 MHz,  $\text{CD}_3\text{NO}_2$ , 300 K) of (a) **1a**·OTf and **1b**·OTf, and (b) the partial exchange of the triflate anion in the salt metathesis reaction between **1a**·OTf and **1b**·OTf, and NaBARf. The  $\text{BARf}^-$  resonances are denoted by the asterisks (\*).

### S2.2.7 Spectroscopic data for 2-BaRF

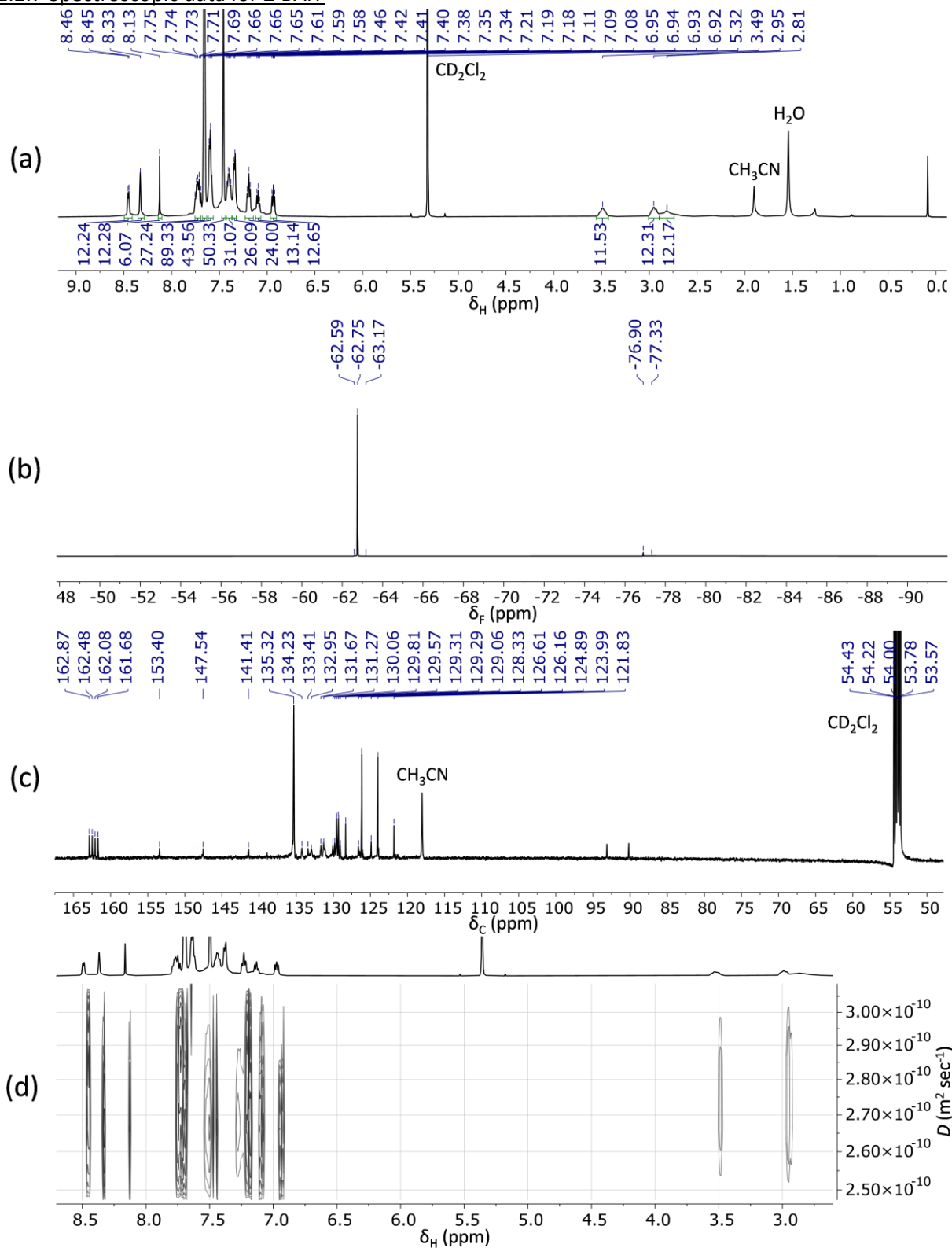


**Figure S2.2.7** (a)  $^1\text{H}$  NMR spectrum ( $\text{CD}_2\text{Cl}_2$ , 500 MHz), (b)  $^{19}\text{F}$  NMR spectrum ( $\text{CD}_2\text{Cl}_2$ , 471 MHz), (c)  $^{13}\text{C}$  NMR spectrum ( $\text{CD}_2\text{Cl}_2$ , 126 MHz), and (d)  $^1\text{H}$  DOSY NMR spectrum ( $\text{CD}_2\text{Cl}_2$ , 500 MHz) of 2-BaRF.

### S3. Mass Spectrometry

Electrospray Ionization (ESI) mass spectra of **1a**-OTf and **1b**-OTf, and **2**-OTf were performed on a Synapt G2 (Waters, Manchester, UK) mass spectrometer, using a direct infusion electrospray ionization source (ESI), controlled using MassLynx S5 v4.1 software. All scans in the experimental are for positive ions. The sample was dissolved in nitromethane or acetonitrile, for **1a**-OTf and **1b**-OTf, and **2**-OTf, respectively, at *ca.* 50  $\mu$ M prior to the measurement. Capillary voltages were adjusted between 1.5 and 2.5 kV to optimize spray quality, while the sampling cone and the extraction cone voltage were minimised to reduce breakdown of the assemblies. Source temperature was set at 80  $^{\circ}$ C. The data was analysed using the MassLynx v4.1 software, with predicted isotopic distributions calculated using mMass open source mass spectrometry tool.<sup>2</sup>

#### S3.1 Spectroscopic data for **1a**-OTf and **1b**-OTf

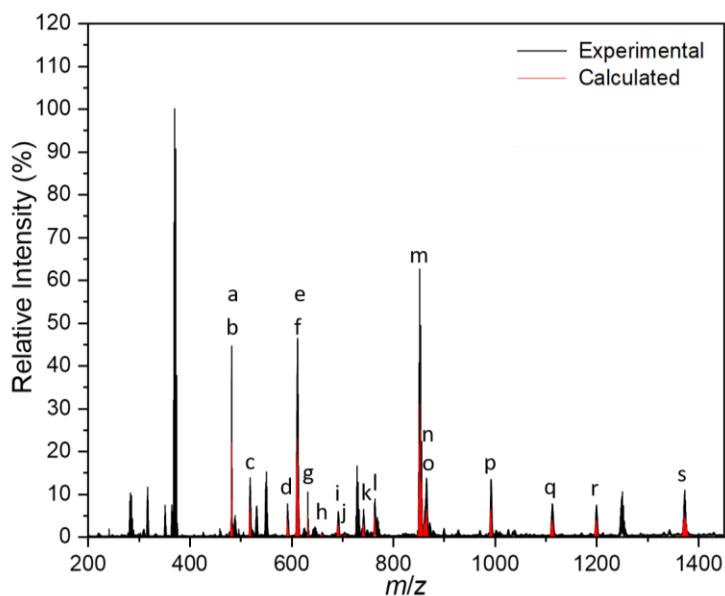


**Figure S3.1.1** ESI-mass spectrum of **1a**-OTf and **1b**-OTf in nitromethane, with experimental (black) and theoretical (red) values. The assignment of the corresponding molecular species are described in Figure S3.1.2.

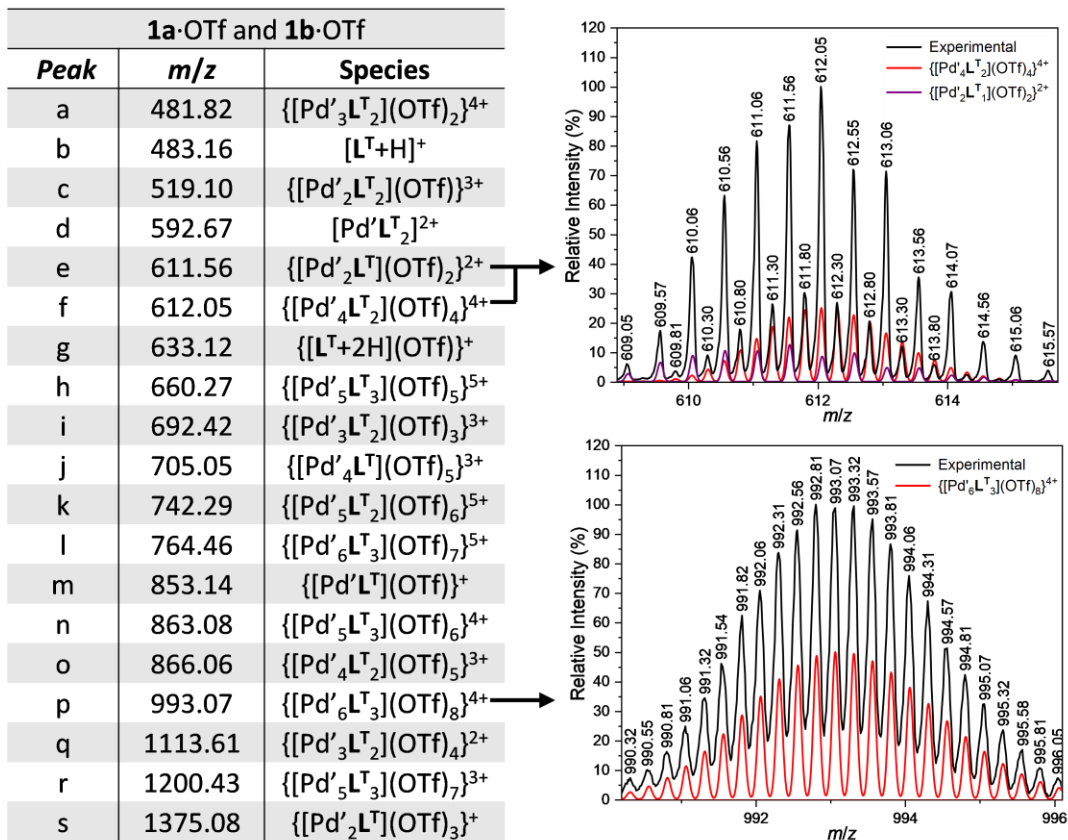


**Figure S3.1.2** The corresponding molecular species for Figure S3.1.1. The isotopic distribution of the  $\{[\text{Pd}'_4\text{L}'_2](\text{OTf})_4\}^{4+}$  and  $\{[\text{Pd}'_6\text{L}'_3](\text{OTf})_8\}^{4+}$  molecular species are shown with the experimental (black) and theoretical (red and purple) values.

### S3.2 Spectroscopic data for 2·OTf

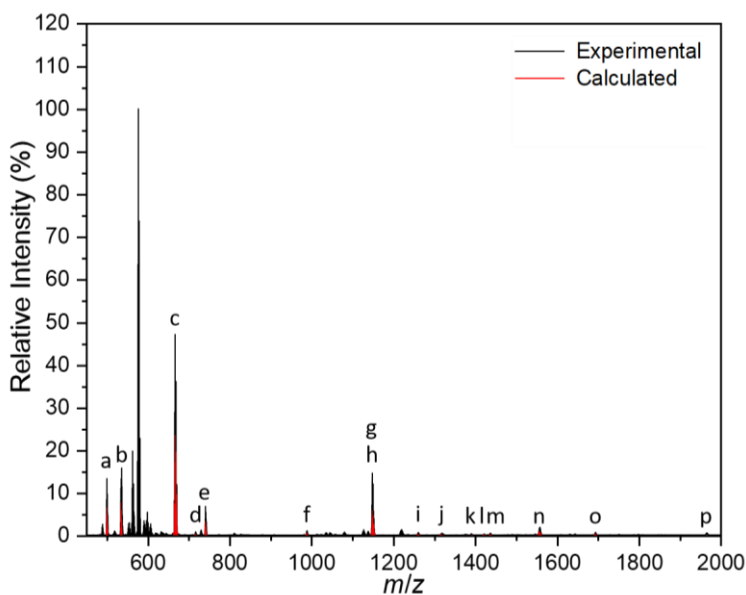


**Figure S3.2.1** Full mass spectrum of the 2·OTf in acetonitrile, with experimental (black) and theoretical (red) values. The assignment of the corresponding molecular species are described in Figure S3.2.2.

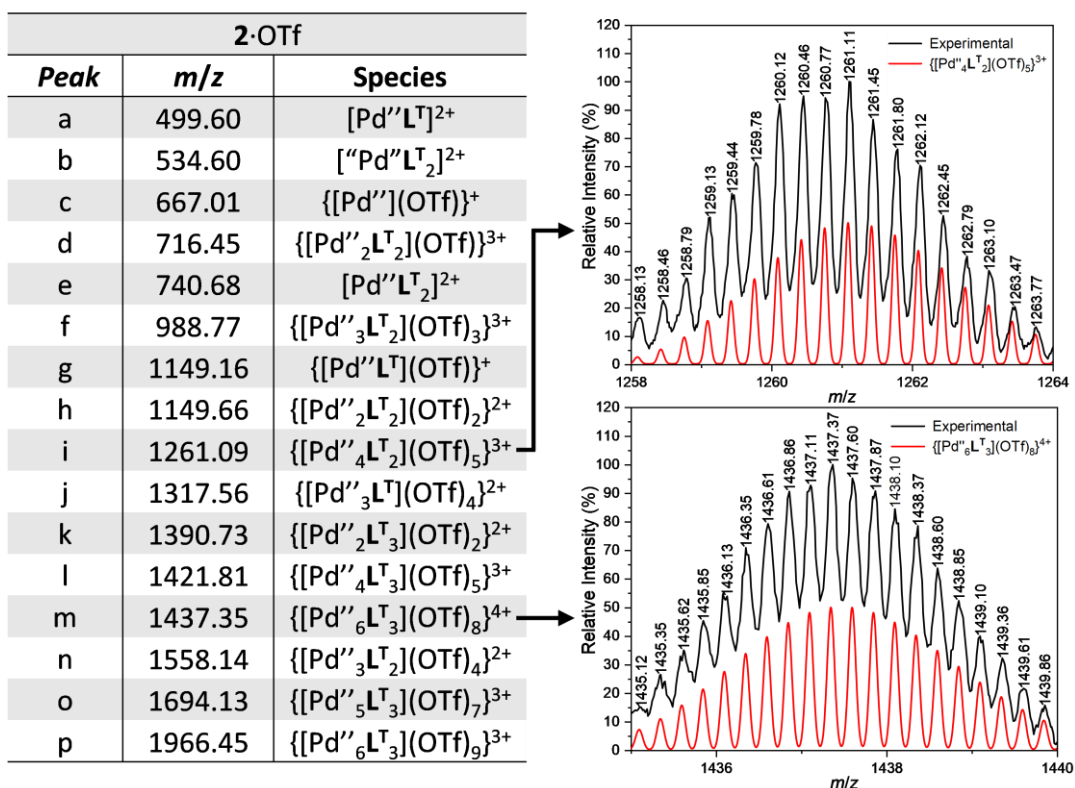


**Figure S3.2.2** The corresponding molecular species for Figure S3.2.1. The isotopic distribution of the  $\{[Pd''_4L^T]_2(OTf)_5\}^{3+}$  and  $\{[Pd''_6L^T]_3(OTf)_8\}^{4+}$  molecular species are shown with the experimental (black) and theoretical (red) values.

## S4. Crystallographic Data Analysis

### S4.1 Crystallographic data for **L<sup>T</sup>**

$C_{36}H_{26}N_4O_2$ ,  $M_r = 546.61$ , triclinic,  $a = 3.7895(2) \text{ \AA}$ ,  $b = 10.0133(5) \text{ \AA}$ ,  $c = 18.8245(9) \text{ \AA}$ ,  $\alpha = 84.216(4)^\circ$ ,  $\beta = 84.817(4)^\circ$ ,  $\gamma = 79.331(4)^\circ$ ,  $V = 696.50(6) \text{ \AA}^3$ ,  $Z = 1$ ,  $P-1$ ,  $D_c = 1.303 \text{ g cm}^{-3}$ ,  $\mu = 0.654 \text{ mm}^{-1}$ ,  $T = 120.0 \text{ K}$ , 11081 reflections measured, 2887 unique ( $R_{int} = 0.0508$ ) which were used in all calculations,  $wR_2$  (all data) = 0.2339, and  $R_1 [I > 2(I)] = 0.0808$ . CCDC number 2007850.

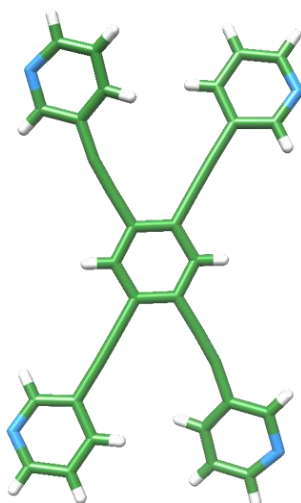


**Figure S4.1** Single X-ray crystal structure of **L<sup>T</sup>**. Solvent molecules of crystallisation have been omitted for clarity. Colour code: C: green, H: white, and N: blue.

### S4.2 Crystallographic data for **1a·OTf**

$C_{116}F_{24}H_{144}N_{16}O_{30}Pd_4S_8$ ,  $M_r = 3380.54$ , monoclinic,  $a = 11.2080(11) \text{ \AA}$ ,  $b = 21.440(2) \text{ \AA}$ ,  $c = 29.333(3) \text{ \AA}$ ,  $\alpha = 90^\circ$ ,  $\beta = 93.016(3)^\circ$ ,  $\gamma = 90^\circ$ ,  $V = 7039.0(12) \text{ \AA}^3$ ,  $Z = 4$ ,  $P2_1/c$ ,  $D_c = 3.190 \text{ g cm}^{-3}$ ,  $\mu = 1.348 \text{ mm}^{-1}$ ,  $T = 100.0 \text{ K}$ , 99311 reflections measured, 14371 unique ( $R_{int} = 0.0626$ ) which were used in all calculations,  $wR_2$  (all data) = 0.2287, and  $R_1 [I > 2(I)] = 0.0664$ . CCDC number 2007851.

### S4.3 Crystallographic data for **2·OTf**

$C_{552}H_{418}F_{72}N_{24}O_{72}P_{24}Pd_{12}S_{24}$ ,  $M_r = 12696.60$ , orthorhombic,  $a = 18.6651(16) \text{ \AA}$ ,  $b = 51.156(4) \text{ \AA}$ ,  $c = 74.909(6) \text{ \AA}$ ,  $\alpha = 90^\circ$ ,  $\beta = 90^\circ$ ,  $\gamma = 90^\circ$ ,  $V = 71526(11) \text{ \AA}^3$ ,  $Z = 4$ ,  $Cmc2_1$ ,  $D_c = 1.179 \text{ g cm}^{-3}$ ,  $\mu = 0.447 \text{ mm}^{-1}$ ,  $T = 100.0 \text{ K}$ , 319787 reflections measured, 38942 unique ( $R_{int} = 0.0842$ ) which were used in all calculations,  $wR_2$  (all data) = 0.1863, and  $R_1 [I > 2(I)] = 0.0623$ . CCDC number 2007852.

S4.4 Comparison of angles between  $L^T$  and 1,3-bis(pyridine-3-ylethynyl)benzene

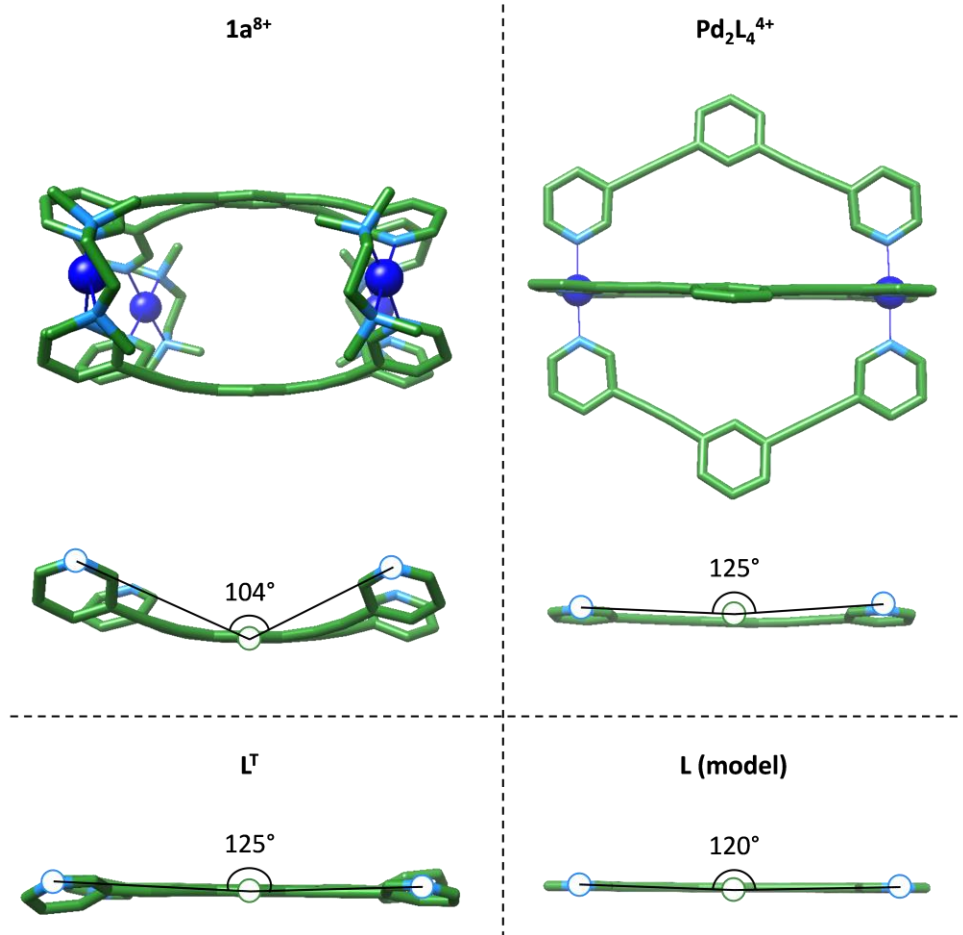


**Figure S4.4** The molecular structures of  $1a^{8+}$  (left) and  $Pd_2L_4^{4+}$  (right). Compared to 1,3-bis(pyridine-3-ylethynyl)benzene, the supposedly rigid  $L^T$  bends and distorts significantly between the two metal ions in the formation of  $1a^{8+}$ . The blue and green circles represent the nitrogen and carbon atoms, respectively, from which the angle is calculated. Colour code: C: green, N: light blue, Pd: blue.

#### S4.5 Additional crystallographic views

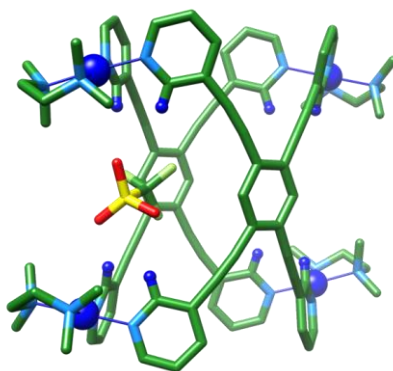


**Figure S4.5.1** X-ray crystal structure of **1a**·OTf as viewed, with respect to the cavities, from the side. Protons and additional counterions have been removed for clarity. Colour code: C: green, N: light blue, O: red, S: yellow, P: orange, Pd: blue, F: light green.

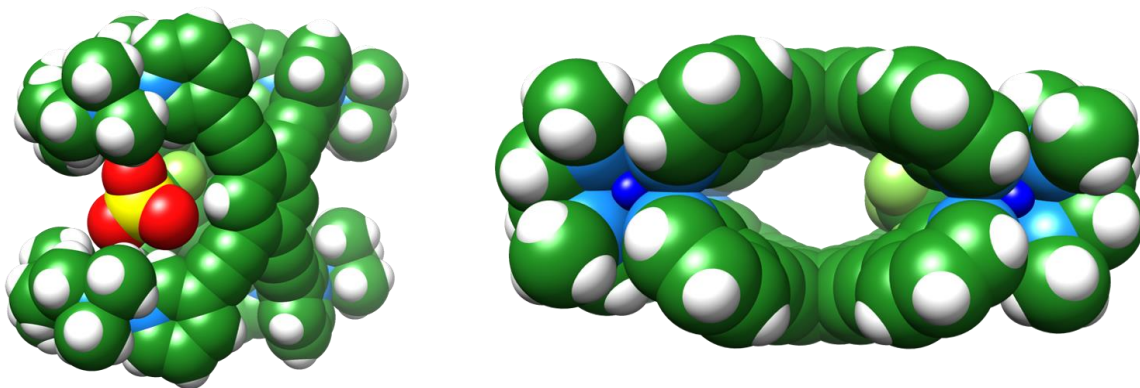


**Figure S4.5.2** Space filling model of **1a**·OTf, as viewed, with respect to the cavities, from the side (left) and top (right). Additional counterions have been removed for clarity. Colour code: C: green, N: light blue, O: red, S: yellow, P: orange, Pd: blue, F: light green.

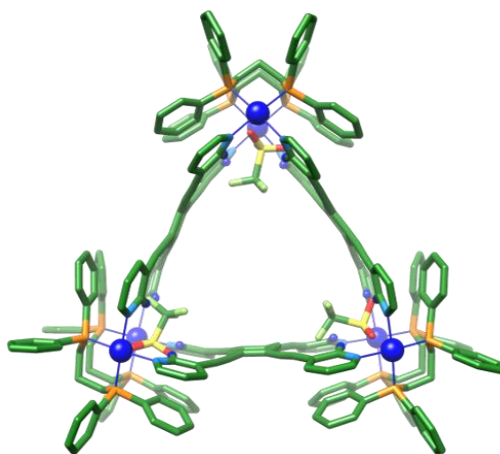


**Figure S4.5.3** X-ray crystal structure of **2**·OTf as viewed, with respect to the cavities, from the top. Protons and additional counterions have been removed for clarity. Colour code: C: green, N: light blue, O: red, S: yellow, P: orange, Pd: blue, F: light green.

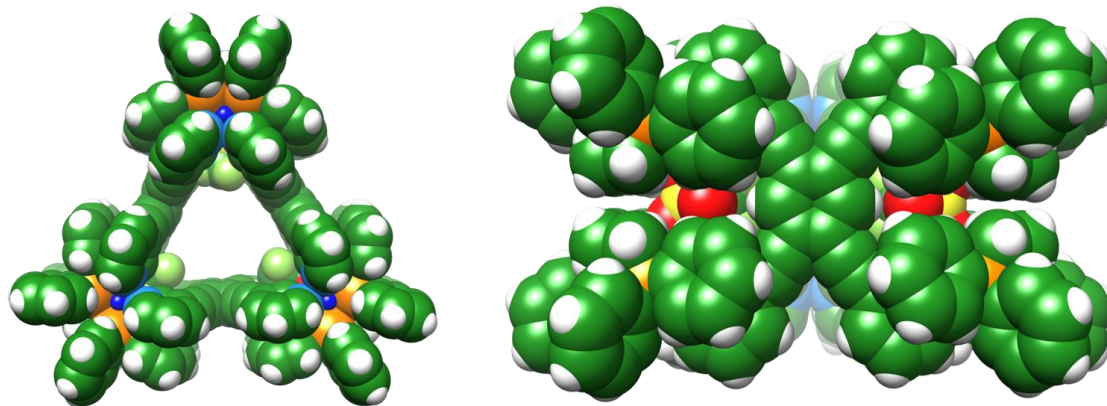


**Figure S4.5.4** Space filling model of **2-OTf** as viewed, with respect to the cavities, from the top (left) and side (right), showing poor access to the triflate binding cavities. Additional counterions have been removed for clarity. Colour code: C: green, N: light blue, O: red, S: yellow, P: orange, Pd: blue, F: light green.

## S4.6 Crystallographic packing

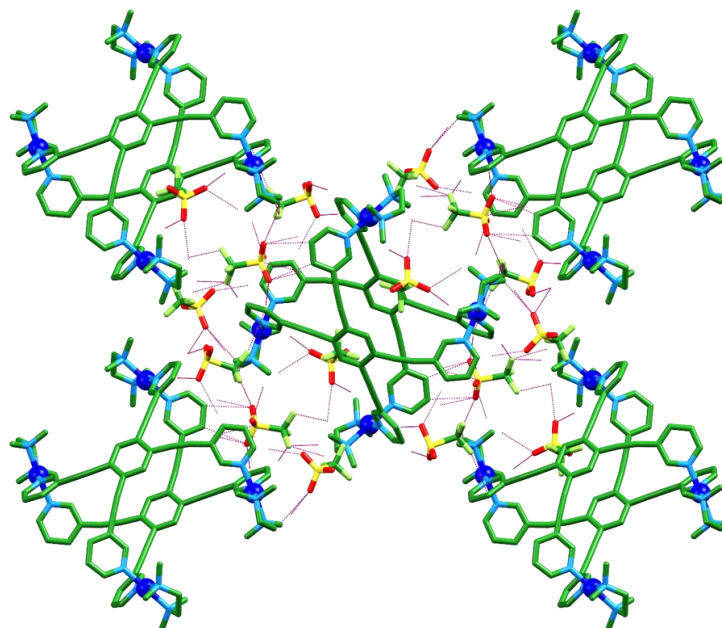


**Figure S4.6.1** The crystal packing of **1a**·OTf as viewed along the *a*-axis. Triflate ions bridge neighbouring metalocycles as shown by numerous short contact interactions (purple dotted lines). Protons and solvent molecules of crystallisation have been removed for clarity. Colour code: C: green, N: light blue, O: red, S: yellow, Pd: blue, F: light green.

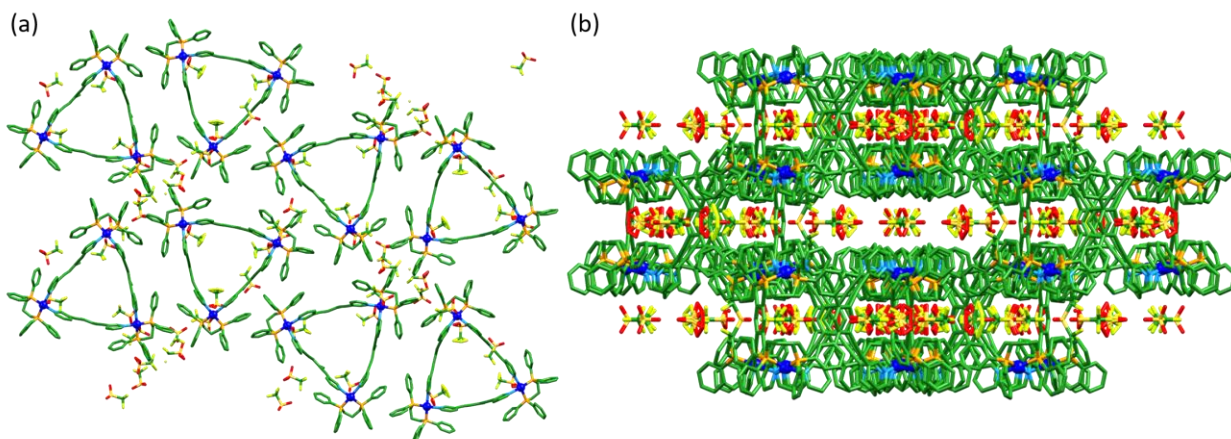


**Figure S4.6.2** The crystal packing of **2**·OTf as viewed along the (a) *a*-axis and (b) *c*-axis. The charge balancing triflate ions are located in the inner and outer pockets of the trigonal prisms, providing close inter-cluster interactions. Protons have been removed for clarity. Colour code: C: green, N: light blue, O: red, S: yellow, P: orange, Pd: blue, F: light green.

#### S4.7 Experimental data for **L<sup>T</sup>**

A suitable crystal  $0.44 \times 0.09 \times 0.04 \text{ mm}^3$  was selected and mounted on a MITIGEN holder in Paratone oil on a Rigaku Oxford Diffraction SuperNova diffractometer. The crystal was kept at a steady  $T = 120.0 \text{ K}$  during data collection. The structure was solved with the ShelXT structure solution program using the Intrinsic Phasing solution method and by using Olex2 as the graphical interface.<sup>3,4</sup> The model was refined with version 2018/3 of ShelXL using Least Squares minimisation.<sup>5</sup> The crystal used exhibits mild pseudo-merohedral twinning, a consequence of the unit cell parameters almost fitting a C-centred monoclinic unit cell. Twin law  $[1\ 0\ 0 / 1\ -1\ 0 / 0\ 0\ -1]$  was applied directly in ShelXL with refined twin scale factor 0.0818(16). The SQUEEZE routine of PLATON was then used to handle electron density pertaining to methanol (two molecules per complete formula unit) which could not be modelled satisfactorily with discrete atoms. This missing solvent is included in the total chemical formula, triggering checkCIF alerts, which should be ignored. One of the pyridyl rings was modelled as disordered over two sites, consistent with displacement ellipsoid behaviour. Geometric similarity restraints were used. The value of  $Z'$  is 0.5. This means that only half of the formula unit is present in the asymmetric unit, with the other half consisting of symmetry equivalent atoms.

#### S4.8 Experimental data for **1a·OTf**

**1a·OTf** crystallised as colourless needle-shaped crystals which desolvated instantly when removed from the mother liquor. Fomblin oil was used to coat a selection of crystals which were then mounted on MiTeGen kapton loops and frozen in liquid nitrogen. The loops were stored in a MiTeGen Unipuck and transported to Diamond Light Source (award CY22240). A crystal with dimensions  $0.42 \times 0.03 \times 0.02 \text{ mm}^3$  was used and data were collected at Diamond Light Source I-19 EH1.<sup>6</sup> The crystal was kept at a steady  $T = 100.0 \text{ K}$  during data collection. The structure was solved with the ShelXT 2018/2 solution program using dual methods and by using Olex2 as the graphical interface. The model was refined with ShelXL 2018/3 using full matrix least squares minimisation on  $F^2$ . The fragment library of Olex2 was used to model the triflate anions, three of which were modelled over two sites consistent with peaks in a difference map.<sup>4</sup> The solvent masking routine of Olex2 was used to handle electron density corresponding with a molecule of diethyl ether which could not be easily modelled with discrete atoms. O-bound H atoms were identified in a difference map and refined with restraints. The value of  $Z'$  is 0.5. This means that only half of the formula unit is present in the asymmetric unit, with the other half consisting of symmetry equivalent atoms.

#### S4.9 Experimental data for **2·OTf**

**2·OTf** crystallised as colourless needle-shaped crystals. This structure was determined using synchrotron radiation on a crystal which desolvated instantly when removed from the mother liquor. Several different attempts to measure data were made before a reasonable data set was obtained. Fomblin oil was used to coat a selection of crystals which were then mounted on MiTeGen kapton loops and frozen in liquid nitrogen. The loops were stored in a MiTeGen Unipuck and transported to Diamond Light Source. Data were collected remotely at beam line I-19 of Diamond Light Source (award CY22240). A crystal with dimensions  $0.42 \times 0.03 \times 0.02 \text{ mm}^3$  was used and data were measured at Diamond Light Source I-19 EH1.<sup>6</sup> The crystal was kept at a steady  $T = 100.0 \text{ K}$  during data collection. The structure was

solved with the ShelXT 2018/2 solution program using dual methods and by using Olex2 as the graphical interface. The model was refined with ShelXL 2018/3 using full matrix least squares minimisation on  $F^2$ .

Crystals of these cage-type compounds tend to suffer from radiation damage. In this case only the first three runs of the data set were used due to the onset of radiation damage from that point onwards. Despite this a complete set of data were measured and cut at a resolution of 1 Å. Choosing the space group was not straightforward. The initial unit cell appeared to be primitive monoclinic with space group P2(1). This gave an asymmetric unit of two complete cages (i.e.  $2 \times \text{Pd}''_6\text{L}_3^{12+}$ ) with an absolute structure parameter of around 0.5. The unit cell could also be re-set as C-centred orthorhombic. Typically, this is 'false' extra symmetry and monoclinic P is the correct setting. In this structure the P2(1) asymmetric unit can be transformed to Cmc2(1) using the ADDSYM function of PLATON. The structure can also be solved independently in Cmc2(1). The structure cannot be solved in Cmcm or indeed any other appropriate higher symmetry space group. This was tested using Superflip, olex2.solve, ShelXS, (direct and Patterson) and ShelXT using the -a and -l switches to explore other space group options. Furthermore, ADDSYM finds no extra symmetry. Thus, the structure is presented in space group Cmc2(1) and refined as an inversion twin with an absolute structure parameter of 0.48(4). The asymmetric unit requires 12 triflate to balance the charges from the cages. The fragment database of Olex2 was used to model triflate anions, based on the shape of peaks in a difference map. Each triflate located lies on a symmetry element. Occupancies were adjusted as appropriate. In total 16 half-triflate anions were identified, a total negative charge of 8- per asymmetric unit. The solvent masking routine of Olex2 accounted for 970 electrons per asymmetric unit. This is presumed to be a mix of additional triflate needed for charge balance and of solvents acetonitrile and diethyl ether. No attempt was made to calculate the amount or proportions of solvent present as this is not indicated at all by the difference map. The missing acetonitrile were added in to correct the formula, which is presented as "+ solvent". The triflate anions were modelled by fitting idealised fragments from the Olex2 fragment library. They were allowed to refine freely for a small number of least squares cycles, with geometric restraints, and then were constrained for the remainder of the refinement. Such constraints were needed to control the ellipsoids of the F and O atoms, particularly the F atoms, which are disordered across a symmetry element and in truth ought to be modelled as a (symmetric) torus of density rather than with discrete atoms. Atom occupancies were adjusted to account for the symmetry (some symmetry-related F are explicitly shown, with half occupancy, for example). RIGU restraint was used on each chemically discrete species, including the cages. Phenyl rings could all be identified from a difference map, but many did not refine cleanly. The AFIX 66 constraint was used to control each of the phenyl rings. Some other geometric similarity restraints were used, particularly on the carbon-carbon triple bonds and some P-CH<sub>2</sub>-CH<sub>2</sub>-CH<sub>2</sub>-P links. The value of Z' is 0.5. This means that only half of the formula unit is present in the asymmetric unit, with the other half consisting of symmetry equivalent atoms. The Flack parameter was refined to 0.47(3). Determination of absolute structure using Bayesian statistics on Bijvoet differences using the Olex2 results in 0.492(8).

#### S4.10 Effect of concentration on the growth of single crystals of 2-OTf

Solutions of 2-OTf were prepared in acetonitrile at concentrations ranging from 0.2 to 0.5 mM. The solutions were sonicated for five minutes before they were filtered. Volumes ranging from 0.5 to 1.0 mL were placed into a 1.7 mL vial. The vials were placed into 14 mL screwcap vials wherein the antisolvent (diethyl ether, 7 mL) was added ensuring no contact with the solutions of 2-OTf. The solutions were left undisturbed for seven days after which time they were examined for the formation of X-ray quality single crystals. The results obtained are shown below in Figure S4.9.



Crystal dimensions  
 $\approx 0.27 \times 0.03 \times 0.01 \text{ mm}^3$

Concentration too high

Concentration too low

Concentration (mM)	Volume of 2-OTf added (mL)		
	0.50	0.75	1.00
0.5	Red	Red	Red
0.4	Red	Green	Green
0.3	Red	Red	Green
0.2	White	White	Red

 = Formation of single X-ray crystallography quality crystals

 = Formation of polycrystalline material

 = No formation of crystalline material

**Figure S4.10** The concentrations used in the attempt to grow single crystals. Only a narrow range of concentrations produced crystals of single X-ray crystallography quality (green). Other concentrations resulted in polycrystalline materials (red) or no formation of crystalline material (white).

## S5. Molecular Modelling

Molecular modelling was performed using Spartan '10 V1.1.0 using an LACVP split basis set. N-Pd-N angles were fixed to 90° and molecular modelling was carried out using a standard 6-31G\* basis set. For the determination of the maximum diameter  $D_{max}$ , in pywindow, all guests, ions and solvent molecules were removed from the X-ray crystal structures **1a**·OTf and **2**·OTf.<sup>7</sup> Helium atoms denote the centre of mass from which the maximum diameter is determined.

### S5.1 Molecular models for TMEDA-based species

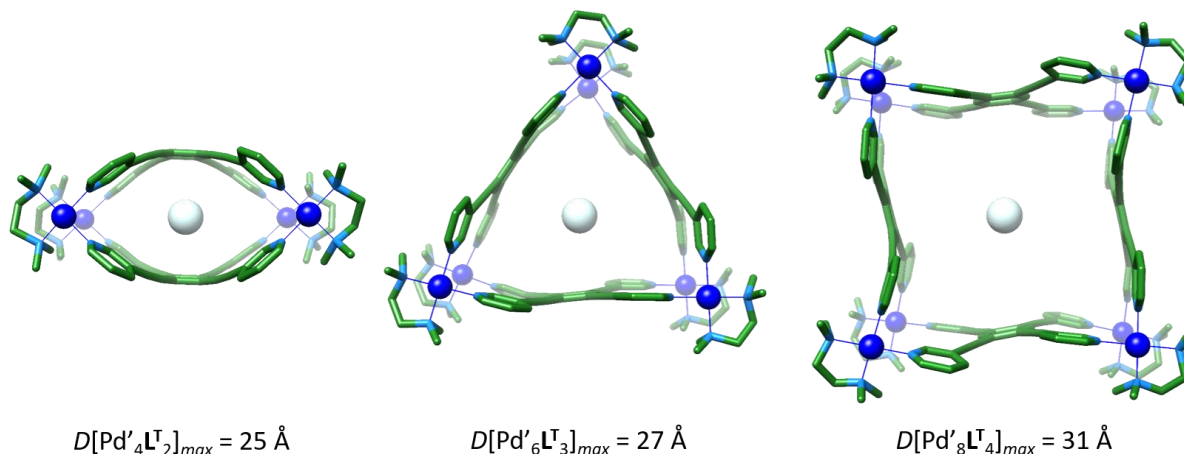


**Figure S5.1** Molecular models of the TMEDA-based  $\text{Pd}'_4\text{L}'_2$ ,  $\text{Pd}'_6\text{L}'_3$ , and  $\text{Pd}'_8\text{L}'_4$  structures, with calculated  $D_{max}$  values. The centre of mass of each structure is denoted by the helium atom. Colour code: C: green, N: light blue, Pd: blue, He: white.

### S5.2 Molecular models for dppp-based species

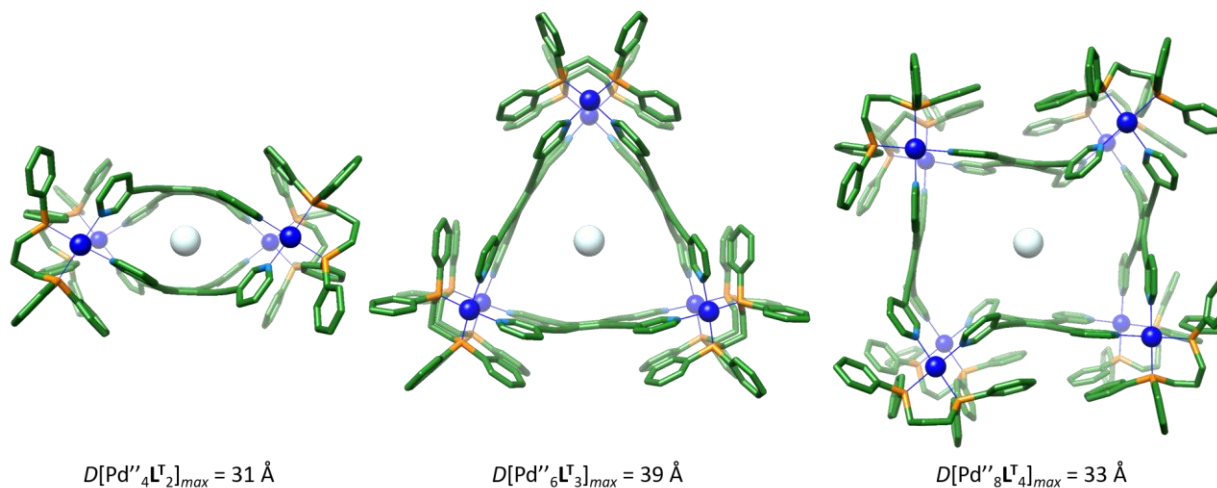


**Figure S5.2** Molecular models of the dppp-based  $\text{Pd}''_4\text{L}''_2$ ,  $\text{Pd}''_6\text{L}''_3$ , and  $\text{Pd}''_8\text{L}''_4$  structures, with calculated  $D_{max}$  values. The centre of mass of each structure is denoted by the helium atom. Colour code: C: green, N: light blue, P: orange, Pd: blue, He: white.

## S6. Host-Guest Studies

$^1\text{H}$  NMR host-guest studies were performed on a 500 MHz Bruker AV III equipped with a DCH cryo-probe (Ava500) at 300 K. Initial sample volumes were 500  $\mu\text{L}$  with a *ca.* 0.50 mM concentration of **2**-BARF in  $\text{CD}_2\text{Cl}_2$ . The guests were added in excess as solids and the tubes sonicated for 5 minutes before  $^1\text{H}$  NMR spectra were recorded.

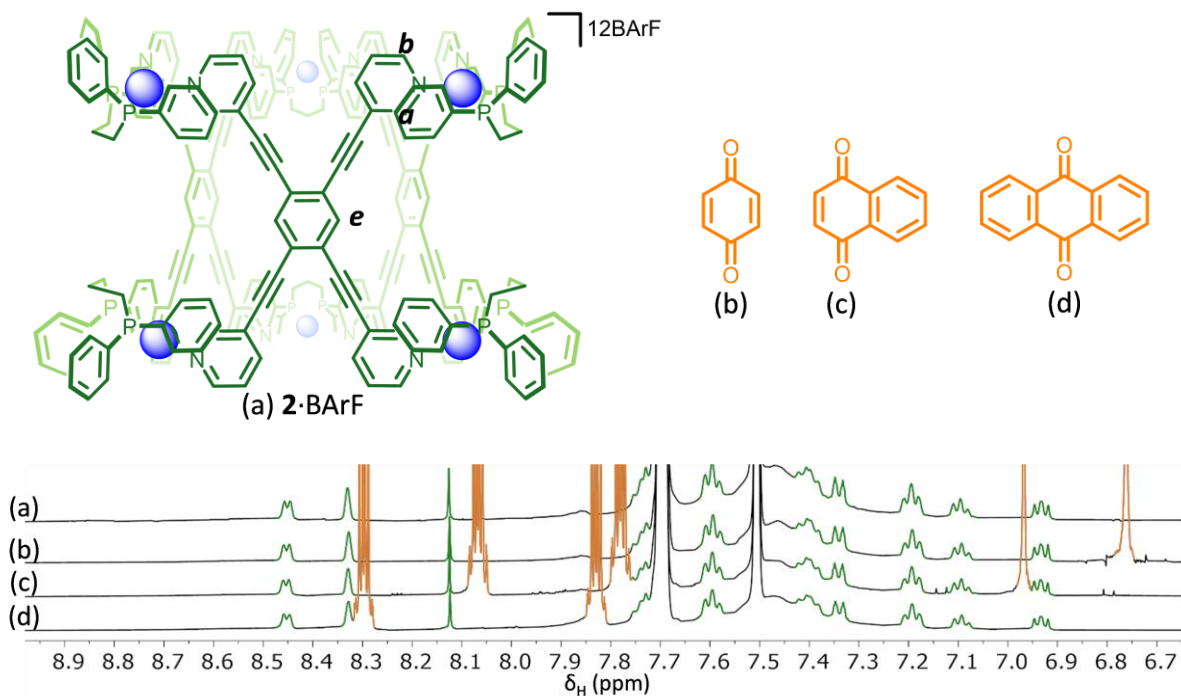


**Figure S6.1**  $^1\text{H}$  NMR host-guest spectra (500 MHz,  $\text{CD}_2\text{Cl}_2$ , 300 K) of (a) **2**-BARF with (b) benzoquinone, (c) naphthoquinone, (d) anthraquinone. The **2**-BARF and guest signals are represented by the green and orange colours, respectively.

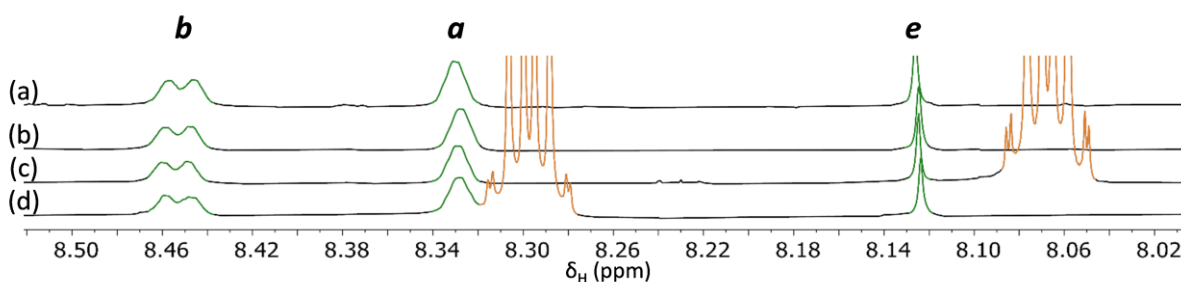


**Figure S6.2**  $^1\text{H}$  NMR host-guest spectra (500 MHz,  $\text{CD}_2\text{Cl}_2$ , 300 K) showing the shifting of peaks *a*, *b*, and *e* of (a) **2**-BARF on the addition of (b) benzoquinone, (c) naphthoquinone, (d) anthraquinone. The **2**-BARF and guest signals are represented by the green and orange colours, respectively.

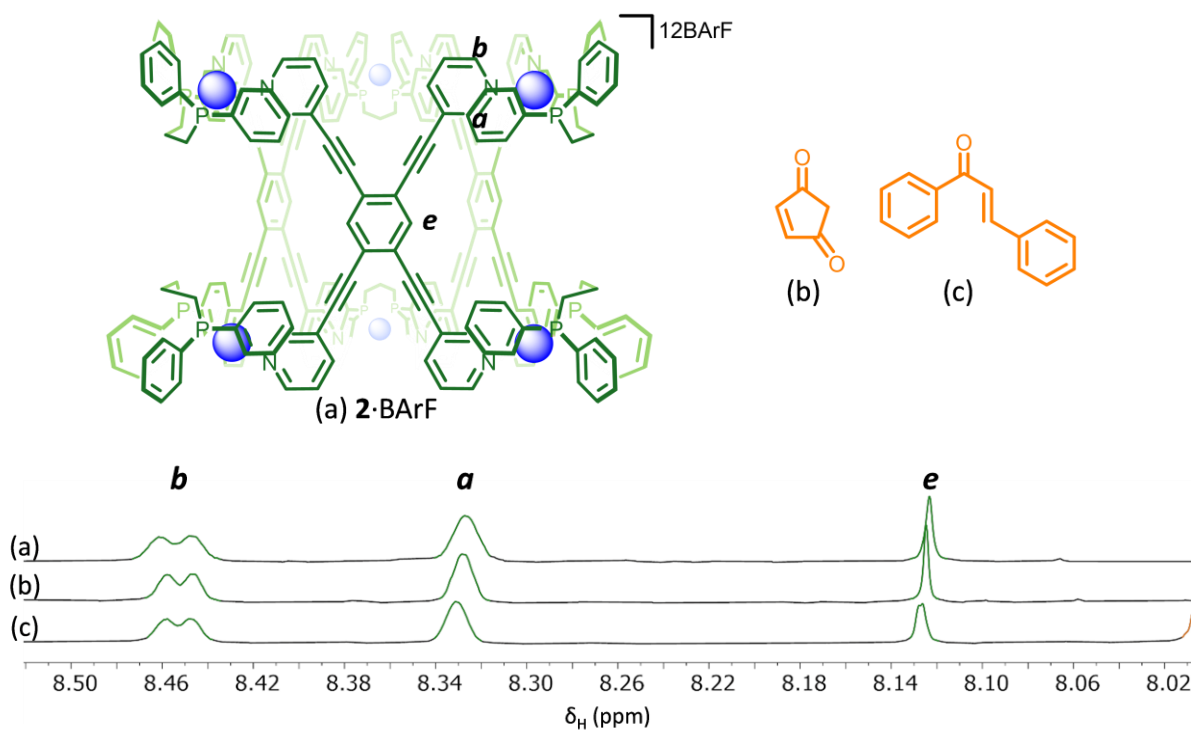


**Figure S6.3** <sup>1</sup>H NMR host-guest spectra (500 MHz, CD<sub>2</sub>Cl<sub>2</sub>, 300 K) showing the shifting of peaks *a*, *b*, and *e* of (a) **2-BArF** with (b) 4-cyclopentene-1,3-dione and (c) chalcone. The **2-BArF** and guest signals are represented by the green and orange colours, respectively.

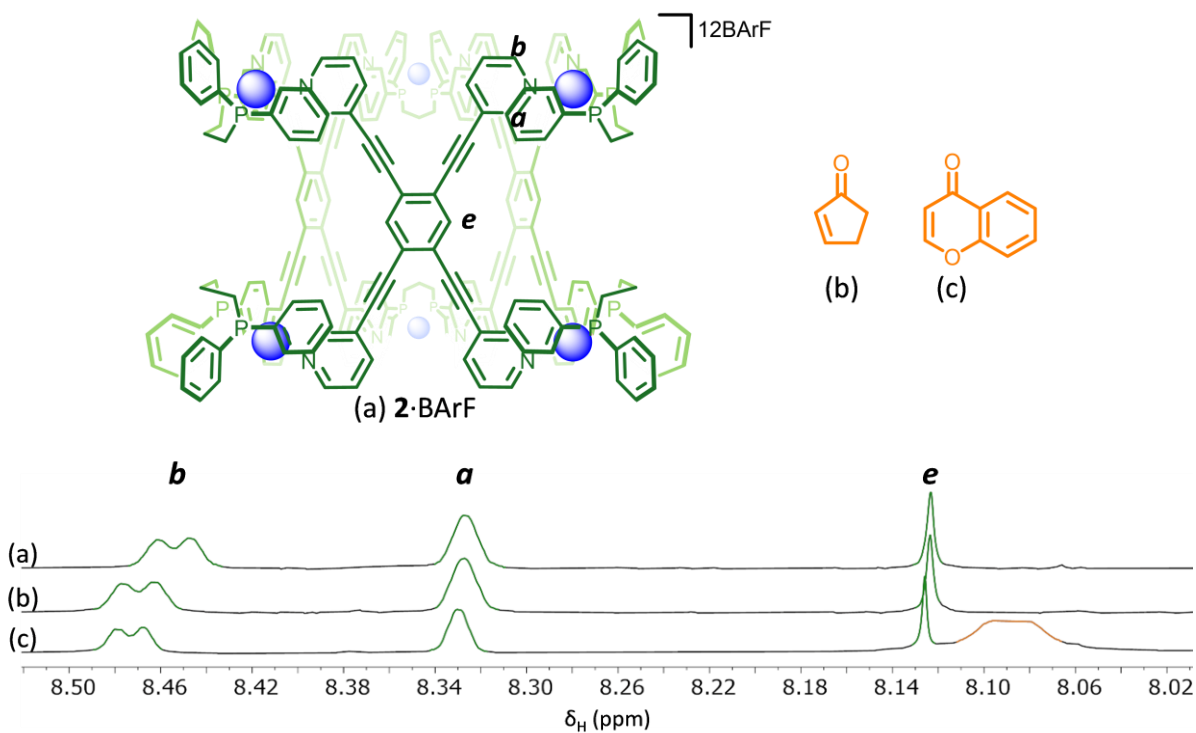


**Figure S6.4** <sup>1</sup>H NMR host-guest spectra (500 MHz, CD<sub>2</sub>Cl<sub>2</sub>, 300 K) showing the shifting of peaks *a*, *b*, and *e* of (a) **2-BArF** with (b) 2-cyclopenten-1-one and (c) chromone. The **2-BArF** and guest signals are represented by the green and orange colours, respectively.

## S7. References

- 1 M. R. Biscoe, B. P. Fors and S. L. Buchwald, *J. Am. Chem. Soc.*, 2008, **130**, 6686-6687.
- 2 M. Strohalm, D. Kavan, P. Novák, M. Volný and V. Havlíček, *Anal. Chem.*, 2010, **82**, 4648-4651.
- 3 G. M. Sheldrick, *Acta Crystallogr. Sect. A Found. Adv.*, 2015, **71**, 3-8.
- 4 O. V. Dolomanov, L. J. Bourhis, R. J. Gildea, J. A. K. Howard and H. Puschmann, *J. Appl. Crystallogr.*, 2009, **42**, 339-341.
- 5 G. M. Sheldrick, *Acta Crystallogr. Sect. C Struct. Chem.*, 2015, **71**, 3-8.
- 6 N. T. Johnson, P. G. Waddell, W. Clegg and M. R. Probert, *Crystals*, 2017, **7**, 360-369.
- 7 M. Miklitz and K. E. Jelfs, *J. Chem. Inf. Model.*, 2018, **58**, 2387-2391.